

EAD: an ensemble approach to detect adversarial examples from the hidden features of deep neural networks

Francesco Craighero¹, Fabrizio Angaroni¹, Fabio Stella¹, Chiara Damiani², Marco Antoniotti^{1,3}, and Alex Graudenzi^{3,4,†}

¹Dept. of Informatics, Systems and Communication, Univ. of Milan-Bicocca, Milan, Italy

²Dept. of Biotechnology and Biosciences, Univ. of Milan-Bicocca, Milan, Italy

³Bicocca Bioinformatics Biostatistics and Bioimaging Centre – B4, Milan, Italy

⁴Inst. of Molecular Bioimaging and Physiology, Consiglio Nazionale delle Ricerche (IBFM-CNR), Segrate, Milan, Italy

[†]Corresponding author

f.craighero@campus.unimib.it, alex.graudenzi@ibfm.cnr.it

{fabrizio.angaroni, fabio.stella, chiara.damiani, marco.antoniotti}@unimib.it

Abstract

One of the key challenges in Deep Learning is the definition of effective strategies for the detection of adversarial examples. To this end, we propose a novel approach named Ensemble Adversarial Detector (EAD) for the identification of adversarial examples generated via benchmark attacks, in a standard multiclass classification scenario. EAD combines multiple detectors that exploit distinct properties of the input instances in the internal representation of a pre-trained Deep Neural Network (DNN), i.e. the hidden layers activations. Specifically, EAD integrates state-of-the-art detectors based on Mahalanobis distance and on Local Intrinsic Dimensionality (LID) with a newly introduced method based on One-class Support Vector Machines (OSVMs). Although all these methods assume that the greater the distance of a test instance from the set of correctly classified training instances, the higher its probability to be an adversarial example, they differ in the way such distance is computed. In order to exploit the effectiveness of the different methods in capturing distinct properties of data distributions and, accordingly, efficiently tackle the trade-off between generalization and overfitting, EAD employs detector-specific distance scores as features of a logistic regression classifier, after independent hyperparameters optimization. We evaluated the EAD approach on distinct benchmark datasets (CIFAR-10, CIFAR-100 and SVHN), different network architectures (ResNet and DenseNet) and with respect to 4 adversarial attacks (FGSM, BIM, DeepFool and CW), also by comparing with competing approaches. Overall, we show that EAD achieves the best AUROC and AUPR in the large majority of the settings, respectively, and comparable performance in the others. The improvement over the state-of-the-art, and the possibility

to easily extend EAD to include any arbitrary set of detectors, pave the way to widespread adoption of ensemble approaches in the broad field of adversarial example detection.

1 Introduction

Deep Neural Networks (DNNs) have achieved remarkable results in complex machine learning tasks, in a variety of fields such as computer vision [1, 2], speech recognition [3], natural language processing [4, 5], gaming [6, 7] and computational biology [8, 9], among others.

However, recent studies have shown that state-of-the-art DNNs for object recognition tasks are vulnerable to *adversarial examples* [10, 11]. For instance, in the field of computer vision, adversarial examples are perturbed images that are misclassified by a given DNN, even if being almost indistinguishable from the original (and correctly classified) image. Adversarial examples have been investigated in many additional real-world applications and settings, including malware detection [12], speech recognition [13] and life sciences [14].

Thus, understanding and countering adversarial examples has become a crucial challenge for the widespread adoption of DNNs in safety-critical settings, and resulted in the development of an ever-growing number of *defensive techniques*. Among the possible countermeasures, some aims at increasing the robustness of the DNN model during the training phase, via *adversarial training* [10, 11, 15] or *defensive distillation* [16] (sometimes referred to as *proactive* methods). Alternative approaches aim at *detecting* adversarial examples in the test phase, by defining specific functions for their detection and filtering-out (*reactive* methods; §2).

Contribution. In this paper, we introduce a novel *ensemble approach* for the detection of adversarial examples, named **Ensemble Adversarial Detector (EAD)**, which integrates scoring functions computed from multiple detectors that process the hidden layer activation of pre-trained DNNs. The underlying rationale is that, given the high-dimensionality of the hidden layers of Convolutional Neural Networks (CNNs) and the hardness of the adversarial detection problem, different algorithmic strategies might be effective in capturing and exploiting distinct properties of adversarial examples. Accordingly, their combination might allow one to better tackle the classical trade-off between generalization and overfitting, outperforming single detectors, as already suggested in [17] in the distinct context of outlier identification. To the best of our knowledge, this is the first time that an ensemble approach is applied to the hidden features of DNNs for adversarial detection.

In detail, EAD includes two state-of-the-art detectors, based on Mahalanobis distance [18] and Local Intrinsic Dimensionality (LID) [19], and a newly developed detector based on One-Class SVMs (OCSVMs) [20]. OCSVMs were previously adopted for adversarial detection in [21], but we improve the previous method by defining both a pre-processing step and a Bayesian hyperparameter optimization strategy (§3.4), both of which result fundamental to achieve performances comparable to [19, 18]. A schematic depiction of the EAD framework is provided in Figure 1.

The performance of EAD and competing methods was assessed with the setting proposed in [18] for the sake of reproducibility and, in particular, we performed experiments with two models, namely ResNet [22] and DenseNet [23], trained on CIFAR-10 [24], CIFAR-100 [24] and SVHN [25]. With regard to adversarial examples generation, we considered four methods: FGSM [11], BIM [26], DeepFool [27] and CW [28].

2 Background

Notation Let us consider a multiclass classification problem with $C > 2$ classes. Let $\mathcal{N}(\mathbf{x}) = \sigma_{\text{tgt}} \circ h_L \circ \dots \circ h_1(\mathbf{x})$ be a DNN with L layers, where h_l is the l^{th} hidden layer and σ_{tgt} is the output layer, i.e. the C logits. To ease the notation, we refer to the activation of the l^{th} hidden layer given the input example \mathbf{x} , i.e. to $h_l \circ \dots \circ h_1(\mathbf{x})$, as $h_l(\mathbf{x})$ and to the logits as $\sigma_{\text{tgt}}(\mathbf{x})$. Let $\sigma_{\text{sm}}(\mathbf{x}) = \sigma_{\text{sm}}(\sigma_{\text{tgt}}(\mathbf{x}))$ be the softmax of $\sigma_{\text{tgt}}(\mathbf{x})$, then the predicted class is $\hat{y} = \arg \max_k \sigma_{\text{sm}}(\mathbf{x})^k$ with confidence $\hat{p} = \max_k \sigma_{\text{sm}}(\mathbf{x})^k$. Lastly, by $J(\mathbf{x}, t) = -\log \sigma_{\text{sm}}(\mathbf{x})^t$ we will denote the cross-entropy loss function given input \mathbf{x} and target class t .

State of the art Let us consider a classifier \mathcal{N} trained on a training set $\mathcal{X}^{\text{train}}$ and a test example $\mathbf{x}_0 \in \mathcal{X}^{\text{test}}$, with

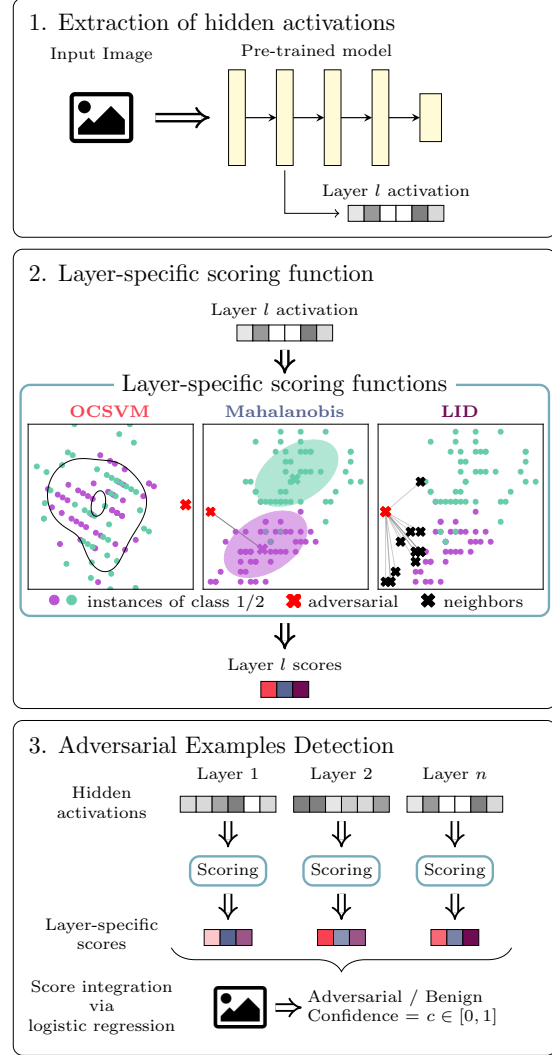


Figure 1: **EAD framework.** A schematic depiction of the EAD framework is displayed. Given an input image and a pre-trained model, in step (1) the hidden activations of each layer are extracted. In order to measure the distance of the image with respect to training examples, in step (2) layer-specific scores are computed via functions based either on One-class Support Vector Machines, Mahalanobis distance [18] or Local Intrinsic Dimensionality [19]. In step (3), the layer- and detector-specific scores are integrated, so to classify the image as benign or adversarial, with a confidence c .

predicted label \hat{y}_0 . Adversarial examples detectors can be broadly categorized according to the considered features: (i) the features of the test example \mathbf{x}_0 , (ii) the hidden features $h_l(\mathbf{x}_0)$, or (iii) the features of the output of the network $out(\mathbf{x}_0)$, i.e. the logits $\sigma_{\text{tgt}}(\mathbf{x}_0)$ or the confidence scores $\sigma_{\text{sm}}(\mathbf{x}_0)$.

In brief, the first family of detectors tries to distinguish normal from adversarial examples by focusing on the input

data. For instance, in [29] the coefficients of low-ranked principal components of \mathbf{x}_0 are used as features for the detector. In [30], the authors employed the statistical divergence, such as Maximum Mean Discrepancy, between \mathcal{X}^{train} and \mathcal{X}^{test} to detect the presence of adversarial examples in \mathcal{X}^{test} .

The second family of detectors aims at exploiting the information of the hidden features $h_l(\mathbf{x}_0)$. In this group, some detectors rely on the identification of the nearest neighbors of $h_l(\mathbf{x}_0)$ to detect adversarial examples, by considering either: the Euclidean distance to the neighbors [31], the conformity of the predicted class among the neighbors [32], the Local Intrinsic Dimensionality [19], the impact of the nearest neighbors on the classifier decision [33] or the prediction of a graph neural-network trained on the nearest neighbors graph [34]. In the same category, additional detectors take into account the conformity of the hidden representation $h_l(\mathbf{x}_0)$ to the hidden representation of instances with the same label in the training set, i.e. to $\{h_l(\mathbf{x}_0) : \hat{y}_0 = y, (\mathbf{x}, y) \in \mathcal{X}^{train}\}$, by computing either the Euclidean distance [35] or the Mahalanobis distance [18, 36] to the class means, or the likelihood of a Gaussian Mixture Model (GMM) [37, 38]. Other detectors take the hidden representation $h_l(\mathbf{x}_0)$ itself as a discriminating feature, by training either a DNN [39], a Support Vector Machine (SVM) [40, 41], a One-class Support Vector Machine (OSVM) [21] or by using a kernel density estimate [42]. Additional methods within this family use the hidden representation $h_l(\mathbf{x}_0)$ as feature to train a predictive model m_l . The model m_l either seeks to predict the same C classes of the original classifier [21, 43] or to reconstruct the input data \mathbf{x}_0 from $h_l(\mathbf{x}_0)$ [29, 44]. The detector then classifies \mathbf{x}_0 as adversarial/benign by relying on the confidence of the prediction \hat{y}_0 in the former case, on its reconstruction error in the latter.

The third family of detectors employs the output of the network $out(\mathbf{x}_0)$ to detect adversarial inputs. In this category, some detectors consider the divergence between $out(\mathbf{x}_0)$ and $out(\phi(\mathbf{x}_0))$ where ϕ is a function such as a squeezing function that reduces the features of the input [45], an autoencoder trained on \mathcal{X}^{train} [46], a denoising filter [47], a random perturbation [48, 49], or an operation of erase and restore of random pixels [50]. Some others take the confidence score of the predicted class \hat{y} , that is expected to be lower when the example is anomalous [29, 44, 51]. Lastly, in [52] a DNN detector was trained directly on the logits, whereas in [42] Bayesian uncertainty of dropout DNNs was used as a feature for the detector.

Detectors exist that do not fall within any of the above families, which employ, for instance, the layer-wise norm of the gradients [53] and the consistency of the softmax scores $\sigma_{sm}(\mathbf{x}_0)$ of multiple models [54].

3 Methods

In this section, we illustrate the EAD ensemble approach for adversarial detection, as well as the properties of the scoring functions it integrates, respectively based on OCSVM (Detector A - *new*), Mahalanobis (Detector B) and LID (Detector C), which can also be used as stand-alone detectors. We also describe the adversarial examples generation, the partitioning of the input data and the extraction of the features processed by EAD and stand-alone detectors.

3.1 Adversarial examples and attack algorithms

Several attack algorithms have been proposed to generate adversarial examples [55]. In this work, we used the Fast Gradient Sign Method (FGSM) [11], the Basic Iterative Method (BIM) [26], the DeepFool method [27] and the Carlini & Wagner (CW) attack [56], as in the experimental setting of [18]. The description of the attacks is provided in the Supplementary Material.

3.2 Data partitioning

Let \mathcal{X}^{train} be the training set on which the classifier \mathcal{N} was trained, \mathcal{X}^{test} the test set and $\mathcal{L}_{norm} \subseteq \mathcal{X}^{test}$ the set of correctly classified test instances. Following the setup done in [19, 18], from \mathcal{L}_{norm} we generate (i) a set of noisy examples \mathcal{L}_{noisy} by adding random Gaussian noise, with the additional constraint of being correctly classified, and (ii) a set of adversarial examples \mathcal{L}_{adv} generated via a given attack. We also ensure that \mathcal{L}_{norm} , \mathcal{L}_{noisy} and \mathcal{L}_{adv} have the same size. The set $\mathcal{L} = \mathcal{L}_{norm} \cup \mathcal{L}_{noisy} \cup \mathcal{L}_{adv}$ will be our *labelled dataset*, where the label is *adv* for adversarial examples and *adv* for benign ones. As detailed in the following sections, \mathcal{L} will be split into a training set \mathcal{L}^{train} , a validation set \mathcal{L}^{valid} for hyperparameter tuning and a test set \mathcal{L}^{test} for the final evaluation.

3.3 Feature Extraction

In our experimental setting, $h_l(\mathbf{x})$, with $l \in [1, \dots, L]$, corresponds to either the first convolutional layer or to the output of the l^{th} dense (residual) block of a DNN (e.g. DenseNet or ResNet). As proposed in [18], the size of the feature map is reduced via average pooling, so that $h_l(\mathbf{x})$ has a number of features equal to the number of channels of the l^{th} layer. Detectors A, B, and C and EAD are applied to such set of features, as detailed in the following.

3.4 Detector A: OCSVM

This newly designed detector is based on a standard anomaly detection technique called One-Class SVM

Algorithm 1 OCSVM detector.

Input: Act. h_l of layer l , trainset \mathcal{X}^{train} , labelled set \mathcal{L}

- 1: **for each** l in $1, \dots, L$ **do**
- 2: Centering and PCA-whitening of h_l : h_l^*
- 3: Select best layer-specific parameters $\theta = \{\nu, \gamma\}$
- 4: Fit OCSVM $_l(\theta)$ on $\{h_l^*(\mathbf{x}) : \mathbf{x} \in \mathcal{X}^{train}\}$
- 5: OCSVM $_l(\theta)$ decision function: O_l
- 6: Layer l score of \mathbf{x}_0 : $O_l(\mathbf{x}_0)$
- 7: **end for**
- 8: Scores vector: $\mathbf{O}(\mathbf{x}_0) := [O_1(\mathbf{x}_0), \dots, O_L(\mathbf{x}_0)]$
- 9: Fit *adv* posterior on \mathcal{L}^{train} : $p(adv | \mathbf{O}(\mathbf{x}_0))$
- 10: OCSVM of \mathbf{x}_0 : OCSVM $(\mathbf{x}_0) := p(adv | \mathbf{O}(\mathbf{x}_0))$
- 11: **return** OCSVM

(OCSVM) [20], which belongs to the family of one-class classifiers [57]. One-class classification is a problem in which the classifier aims at learning a good description of the training set and then rejects the inputs that do not resemble the data it was trained on, which represent outliers or anomalies. This kind of classifiers is usually adopted when only one class is sufficiently represented within the training set, while the others are undersampled or hard to be characterized, as in the case of adversarial examples, or anomalies in general. OCSVM was first employed for adversarial detection in [21]. Here, we modified it by defining an input pre-processing step based on PCA-whitening [58], and by employing a Bayesian optimization technique [59] for hyperparameter tuning. The pseudocode is reported in Algorithm 1.

Preprocessing. OCSVM employs a kernel function (in our case a Gaussian RBF kernel) that computes the Euclidean distance among data points. Hence, it might be sound to standardize all the features of the data points, at the preprocessing stage, to make them equally important. To this end, each hidden layer activation $h_l(\mathbf{x}_0)$ is first centered on the mean activations $\mu_{l,c}$ of the examples of the training set \mathcal{X}^{train} of class c . Then, PCA-whitening \mathbf{W}_l^{PCA} is applied:

$$\begin{aligned} h_l^*(\mathbf{x}_0) &= \mathbf{W}_l^{PCA} \cdot (h_l(\mathbf{x}_0) - \mu_{l,c}) \\ &= \mathbf{\Lambda}_l^{-1/2} \cdot \mathbf{U}_l^T \cdot (h_l(\mathbf{x}_0) - \mu_{l,c}), \end{aligned}$$

where \mathbf{U}_l^T is the eigenmatrix of the covariance Σ_l of activations h_l and $\mathbf{\Lambda}_l$ is the eigenvalues matrix of the examples of \mathcal{X}^{train} . Whitening is a commonly used preprocessing technique for outlier detection, since it enhances the separation of points that deviate in low-variance directions [60]. Moreover, in [36] it was conjectured that the effectiveness of the Mahalanobis distance [18] for out-of-distribution and adversarial detection is due to the strong contribution of low-variance directions. Thus, this preprocessing step allows the

one-class classifier to achieve better overall performances¹.

Layer-specific scoring function. After preprocessing, a OCSVM with a Gaussian RBF kernel is trained on the hidden layer activations h_l of layer l of the training set \mathcal{X}^{train} . Once the model has been fitted, for each instance \mathbf{x}_0 layer-specific scores $\mathbf{O}(\mathbf{x}_0) = [O_1(\mathbf{x}_0), O_2(\mathbf{x}_0), \dots, O_L(\mathbf{x}_0)]$ are evaluated. More in detail, let S_l be the set of support vectors, the decision function $O_l(\mathbf{x}_0)$ for the l^{th} layer is computed as:

$$O_l(\mathbf{x}_0) = \sum_{sv \in S_l} \alpha_{sv} k(h_l(\mathbf{x}_0), sv) - \rho, \quad (1)$$

where α_{sv} is the coefficient of the support vector sv in the decision function, ρ is the intercept of the decision function and k is a Gaussian RBF kernel with kernel width γ :

$$k(\mathbf{x}, \mathbf{y}) = \exp\left(-\gamma \|\mathbf{x} - \mathbf{y}\|^2\right). \quad (2)$$

Hyperparameter optimization. The layer-specific scoring function takes two parameters as input: the regularization factor $\nu \in (0, 1)$ that controls the fraction of training errors that should be ignored, and the kernel width γ . This hyperparameters must be carefully chosen to achieve good performances. For this purpose, many approaches have been proposed for hyperparameters selection in OCSVMs [61]. In our setting, we used the validation set of labelled examples \mathcal{L}^{valid} to choose the best combination of parameters, based on the validation accuracy. To avoid a full (and infeasible) exploration of the parameters space, we employed Bayesian hyperparameter optimization, via the *scikit-optimize* library [62].

Adversarial detection. Once the scores have been obtained for each layer, they can serve either as input for the stand-alone detector A or as partial input of the ensemble detector EAD. In the former case, in order to aggregate the scores of the separate layers $\mathbf{O}(\mathbf{x}_0)$, this detector employs a logistic regression to model the posterior probability of adversarial (*adv*) examples:

$$p(adv | \mathbf{O}(\mathbf{x}_0)) = \left(1 + \exp\left(\beta_0 + \beta^T \mathbf{O}(\mathbf{x}_0)\right)\right)^{-1}, \quad (3)$$

The parameters $\{\beta_0, \beta\}$ are fitted with a cross-validated procedure using the labelled training set \mathcal{L}^{train} .

¹In a test on the DenseNet, CIFAR-10, CW scenario, the AUROC returned by the OCSVM detector with PCA-whitening preprocessing improves from 82.56 to 90.24, and the AUPR from 78.17 to 82.98, with respect to the same method without preprocessing (see §4 for further details).

3.5 Detector B: Mahalanobis

The Mahalanobis detector was originally introduced in [18]. The algorithmic procedure is akin to that of the OCSVM detector, and includes a final layer score aggregation step via logistic regression, but it is based on a different layer-specific scoring function.

Layer-specific scoring function. Given a test instance \mathbf{x}_0 , the layer score is computed via a three-step procedure: first, for each instance, the class \hat{c} is selected, such that:

$$\hat{c} = \arg \min_c \text{Maha}_l(\mathbf{x}_0, c),$$

where $\text{Maha}_l(\mathbf{x}, c)$ is the Mahalanobis distance for the l^{th} layer between the activations $h_l(\mathbf{x})$ and the mean values $\mu_{l,c}$ of the examples in the training set $\mathcal{X}^{\text{train}}$:

$$\text{Maha}_l(\mathbf{x}, c) = (h_l(\mathbf{x}) - \mu_{l,c})^T \Sigma_l^{-1} (h_l(\mathbf{x}) - \mu_{l,c}), \quad (4)$$

where Σ_l is the covariance matrix of the examples of $\mathcal{X}^{\text{train}}$ in layer l . Then, the instance is preprocessed to obtain a better separation between benign and adversarial examples similarly to what discussed in [51]:

$$\mathbf{x}_0^* = \mathbf{x}_0 - \lambda \text{sign } \nabla_{\mathbf{x}_0} \text{Maha}_l(\mathbf{x}_0, \hat{c}),$$

where λ is positive real number, called the perturbation magnitude. The scoring for instance \mathbf{x}_0 is computed as:

$$\mathbf{M}(\mathbf{x}_0) = [\mathbf{M}_1(\mathbf{x}_0), \mathbf{M}_2(\mathbf{x}_0), \dots, \mathbf{M}_L(\mathbf{x}_0)],$$

where

$$\mathbf{M}_l(\mathbf{x}_0) = -\max_c \text{Maha}_l(\mathbf{x}_0^*, c).$$

Adversarial detection. The scores can serve either as input for the stand-alone detector B or as partial input of the ensemble detector EAD. In the latter case, the Mahalanobis detector uses a logistic regression to identify adversarial examples, with a procedure similar to that already described for stand-alone detector A.

Hyperparameter optimization. Differently from detector A, the hyperparameter selection is performed downstream of the adversarial detection stage. In order to select the best λ (unique for all layers), the method selects the value that achieves the best Area Under the Receiver Operating Characteristic (AUROC) on $\mathcal{L}^{\text{valid}}$ computed on the posterior probability $p(\text{adv} | \mathbf{M}(\mathbf{x}_0))$, which is obtained via the logistic regression fitted on $\mathcal{L}^{\text{train}}$ (the definition of AUROC is provided in the Supplementary Material).

3.6 Detector C: LID

The third detector uses a procedure similar to detectors A-B, but the layer-specific scoring function is based on the Local Intrinsic Dimensionality (LID) approach [19].

Algorithm 2 EAD detector.

Input: Act. h_l of layer l , trainset $\mathcal{X}^{\text{train}}$, labelled set \mathcal{L}

- 1: Select best hyperparameters for OCSVM, Maha, LID
- 2: **for each** layer l in $1, \dots, L$ **do**
- 3: Layer l scores of \mathbf{x}_0 : $\mathbf{O}_l(\mathbf{x}_0), \mathbf{M}_l(\mathbf{x}_0), \mathbf{L}_l(\mathbf{x}_0)$
- 4: **end for**
- 5: Scores vector: $\mathbf{E}(\mathbf{x}_0) := [\mathbf{O}(\mathbf{x}_0), \mathbf{M}(\mathbf{x}_0), \mathbf{L}(\mathbf{x}_0)]$
- 6: Fit *adv* posterior on $\mathcal{L}^{\text{train}}$: $p(\text{adv} | \mathbf{E}(\mathbf{x}_0))$
- 7: EAD on \mathbf{x}_0 : $\text{EAD}(\mathbf{x}_0) := p(\text{adv} | \mathbf{E}(\mathbf{x}_0))$
- 8: **return** EAD

Layer-specific scoring function. Given a test instance \mathbf{x}_0 , the LID layer-specific scoring function \mathbf{L} is defined as:

$$\mathbf{L}_l(\mathbf{x}_0) = -\left(\frac{1}{k} \sum_{i=1}^k \log \frac{r_i(h_l(\mathbf{x}_0))}{\max_i r_i(h_l(\mathbf{x}_0))}\right)^{-1}, \quad (5)$$

where, k is the number of nearest neighbors, r_i is the Euclidean distance to the i -th nearest neighbor in the set of normal examples $\mathcal{L}_{\text{norm}}$. The layer-specific scores are:

$$\mathbf{L}(\mathbf{x}_0) = [\mathbf{L}_1(\mathbf{x}_0), \mathbf{L}_2(\mathbf{x}_0), \dots, \mathbf{L}_L(\mathbf{x}_0)]$$

Adversarial detection. When considered alone, the LID detector employs a logistic regression to identify adversarial examples, similarly to the other detectors (see above).

Hyperparameter optimization. Similarly to detector B, the hyperparameter selection is performed downstream of the adversarial detection stage. k is selected as the value that achieves the best AUROC on $\mathcal{L}^{\text{valid}}$ computed on the posterior probability $p(\text{adv} | \mathbf{L}(\mathbf{x}_0))$, which is obtained via the logistic regression fitted on $\mathcal{L}^{\text{train}}$. Note that k is unique for all layers.

3.7 Ensemble Adversarial Detector (EAD)

The EAD approach exploits the effectiveness of detectors A, B, and C in capturing different properties of data distributions, by explicitly integrating the distinct layer-specific scoring functions in a unique classification framework. More in detail, given a test instance \mathbf{x}_0 , it will be characterized by a set of layer-specific and detector-specific features, computed from the scoring functions defined above, that is: $\mathbf{E}(\mathbf{x}_0) = [\mathbf{O}(\mathbf{x}_0), \mathbf{M}(\mathbf{x}_0), \mathbf{L}(\mathbf{x}_0)]$. It should be noted that training and hyperparameter optimization is executed for each detector independently.

Adversarial detection. In its current implementation, in order to integrate the scores of the separate layers $\mathbf{E}(\mathbf{x}_0)$,

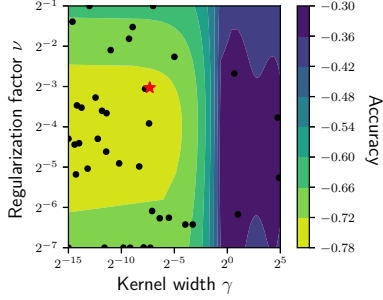


Figure 2: **OCSVM hyperparameter optimization.** The influence of different combinations of OCSVM hyperparameters $\{\nu, \gamma\}$ on the validation accuracy is explored via Bayesian optimization [62], in the example scenario of DenseNet model, CIFAR-10 dataset and DeepFool attack. The gradient returns the validation accuracy estimated on \mathcal{L}^{valid} . The red star represents the optimal configuration, which is then employed for adversarial detection in both the OCSVM and the EAD detectors.

Detector	Parameter	Configurations
OCSVM	ν	$2^{-7}, 2^{-6}, \dots, 2^{-1}$
	γ	$2^{-15}, 2^{-14}, \dots, 2^5$
LID	k	10, 20, \dots , 90
Maha	λ	0.0, 0.01, 0.005, 0.002, 0.0014, 0.001, 0.0005

Table 1: **Hyperparameters configurations.** Hyperparameters space explored in the optimization step for the three detectors OCSVM, LID and Mahalanobis.

EAD employs a simple logistic regression to model the posterior probability of adversarial (*adv*) examples:

$$p(adv | \mathbf{E}(\mathbf{x}_0)) = \left(1 + \exp\left(\beta_0 + \beta^T \mathbf{E}(\mathbf{x}_0)\right)\right)^{-1}. \quad (6)$$

Like detectors A, B, and C, the logistic is fitted with a cross-validation procedure using the labelled training set \mathcal{L}^{train} . Fitting the logistic allows one to have different weights, i.e. the elements of β^T , for the different layers and detectors, meaning that a given detector might be more effective in isolating an adversarial example when processing its activation on a certain layer of the network. The pseudocode is reported in Algo. 2.

4 Results

We compared the performance of EAD with stand-alone detectors A, B, and C. All approaches were tested on 2 networks architectures (ResNet and DenseNet), 3 benchmark datasets (CIFAR-10, CIFAR-100 and SVHN) and 4 adver-

	FGSM	BIM	DeepFool	CW		
CIFAR10	19815	13	24189	104	19046	1172
	114	38	118	429	847	4045
CIFAR100	18435	21	18883	196	13915	864
	60	114	147	484	597	3794
SVHN	27230	78	63144	876	57252	2140
	76	156	766	1634	1683	5345

MO	O
M	Ø

% of total instances

Figure 3: **Comparison of predictions of single detectors.** The contingency table shows the number of adversarial examples correctly identified: by both the OCSVM and the Mahalanobis detectors (OM), by either one of the two methods (O or M), by none of them (\emptyset). The results of the DenseNet model, with respect to the distinct datasets and attacks are shown, whereas the remaining comparisons are displayed in the Supplementary Material.

sarial attacks (FGSM, BIM, DeepFool and CW), for a total of 24 distinct configurations, as originally proposed in [18]. For the evaluation of the performances, we employed two standard threshold-independent metrics, namely AUROC and Area Under Precision Recall (AUPR) [63], which are detailed in the Supplementary Material.

Selected hyperparameters. The hyperparameter optimization was executed separately for detectors A, B and C, by scanning the configurations reported in Table 1. In all tests, the hyperparameter optimization was performed on the \mathcal{L}^{valid} set, whereas the logistic regression fit on the \mathcal{L}^{train} set of the same attack, except for the unknown attack scenario (§4.3), in which both the hyperparameters and the logit weights were estimated on the FGSM attack and employed with the others.

The selected hyperparameters for each experimental setting are shown in Supplementary Tables 1 and 2. In addition, in Figure 2, we report the estimated accuracy of the explored solutions in the specific case of the OCSVM detector, in a representative experimental setting.

4.1 Stand-alone detectors capture distinct properties of adversarial examples

In order to assess the ability of detectors A, B and C to exploit different properties of input instances, we first analyzed the methods as stand-alone, and computed the subsets of adversarial examples identified: (i) by all detectors, (ii) by a subset of them, (iii) by none of them.

In Figure 3, we return a contingency table in which we compare the OCSVM and Mahalanobis detectors on all the

experimental settings with the DenseNet model, while the remaining pairwise comparisons are presented in the Supplementary Material. Importantly, while the class of examples identified by both approaches is, as expected, the most crowded, we observe a substantial number of instances that are identified by either one of the two approaches. This important result appear to be general, as it is confirmed in the other comparisons between stand-alone detectors. In addition, in Supplementary Figures 4 one can find the layer-specific scores returned by all detectors in a specific setting (ResNet, DeepFool, CIFAR-10). For a significant portion of examples, the ranking ordering among scores is not consistent across detectors, confirming the distinct effectiveness in capturing different data properties in the hidden layers.

To investigate the importance of the layers with respect to the distinct attacks, models and datasets, we also computed the AUROC directly on the layer-specific scores, i.e. O_l , M_l and L_l . In Figure 4, one can find the results for all detectors in all settings, with the DenseNet model. For the FGSM attack, the scores computed on the middle layers consistently return the best AUROC in all datasets, while for the BIM attack the last layer is apparently the most important. Notably, with DeepFool and CW attacks the most important layers are dataset-specific. This result demonstrates that each attack may be vulnerable in distinct layers of the network.

4.2 EAD outperforms stand-alone detectors

Table 2 reports the AUROC and AUPR computed on $p(adv | \mathbf{E}(x))$ for EAD, and on $p(adv | \mathbf{O}(x))$, $p(adv | \mathbf{M}(x))$ and $p(adv | \mathbf{L}(x))$, for detectors A, B, and C, respectively, on all 24 experimental settings.

It can be noticed that EAD exhibits both the best AUROC and the best AUPR in 22 out of 24 settings (including 1 tie with OCSVM), with the greatest improvements emerging in the hardest attacks, i.e. DeepFool and CW. Remarkably, the newly designed OCSVM detector outperforms the other stand-alone detectors in 12 and 14 settings in terms of AUROC and AUPR, respectively.

Notice that in Supplementary Table 5, we also evaluated the performance of all pairwise combinations of the three detectors, so to quantitatively investigate the impact of integrating the different algorithmic approaches, proving that distinct ensembles of detectors might be effective in specific experimental settings.

4.3 EAD and OCSVM detectors are robust against unknown attacks

We finally assessed the performance of EAD and detectors A, B, and C when an unknown attack is performed. In detail, we performed the hyperparameters optimization and

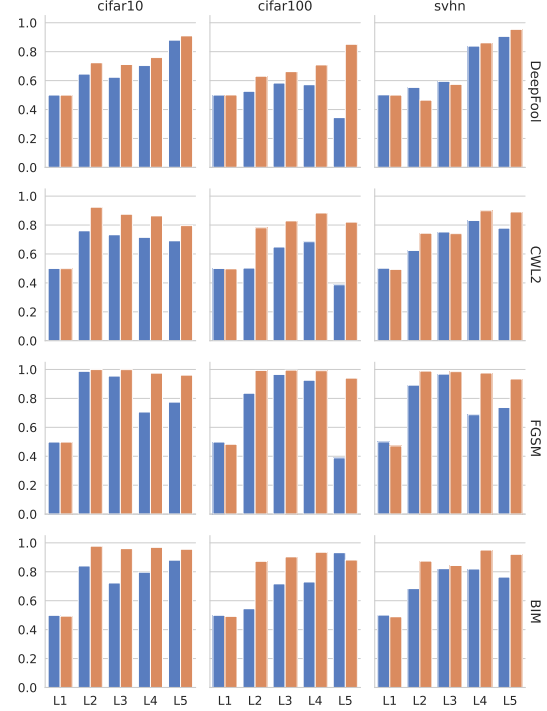


Figure 4: **Influence of layers in adversarial detection.** For each configuration of datasets and attacks on the DenseNet model, the AUROC of each layer-specific score for detectors A–C is returned. For each configuration and detector, the best performing layer is highlighted with a darker shade.

the logit fit on the FGSM attack, for all methods, and then tested the performance on BIM, DeepFool and CW attacks. Despite the expected worsening of the performances, either EAD or OCSVM achieve the best AUROC in all settings (see Table 3), proving their robustness and applicability to the real-world scenarios in which the adversarial example type might be unknown.

5 Limitations

Our tests demonstrate that the application of ensemble approaches to the hidden features of DNNs is a viable and effective option for adversarial detection. However, the current implementation of EAD presents certain limitations.

First, due to the design of its theoretical framework, the computational time of EAD is approximately the sum of that of the detectors employed to compute the layer-specific scores and, in the current version, is mostly affected by OCSVM (see the computation time assessment in Supplementary Figure 2). Therefore, more efficient implementation schemes should be considered to improve the scalability of EAD. Furthermore, one might also want to employ versions of EAD including subsets of computationally ef-

Model	Dataset	Attack Detector	FGSM		BIM		DeepFool		CW	
			AUPR	AUROC	AUPR	AUROC	AUPR	AUROC	AUPR	AUROC
DenseNet	CIFAR-10	LID	96.37	98.30	99.52	99.73	75.21	85.22	69.75	80.88
		Maha	99.80	99.96	99.46	99.75	74.46	82.73	78.43	87.42
		OCSVM	99.58	99.88	99.24	99.69	77.01	84.74	82.98	90.24
		EAD	99.70	99.89	99.90	99.96	83.70	89.36	85.30	91.50
	CIFAR-100	LID	98.39	99.29	96.31	98.11	55.88	70.12	59.67	72.80
		Maha	99.49	99.87	97.64	99.10	67.79	78.49	74.99	86.86
		OCSVM	99.49	99.84	98.23	99.30	69.17	79.27	78.71	88.95
		EAD	99.78	99.93	98.37	99.47	73.05	83.07	83.40	92.15
	SVHN	LID	98.59	99.07	92.13	94.79	85.80	91.83	90.47	94.61
		Maha	99.45	99.85	97.93	99.26	90.00	94.93	90.95	97.16
		OCSVM	99.51	99.86	97.38	99.17	91.40	95.00	96.54	98.50
		EAD	99.83	99.91	98.93	99.57	93.27	96.04	98.13	99.16
ResNet	CIFAR-10	LID	99.18	99.67	94.37	96.50	79.40	88.58	73.95	82.29
		Maha	99.87	99.90	99.06	99.58	85.64	91.60	92.28	95.90
		OCSVM	99.99	99.99	98.95	99.44	83.90	90.83	92.26	95.68
		EAD	99.99	99.99	99.58	99.78	87.77	92.89	93.35	96.46
	CIFAR-100	LID	97.53	98.78	94.52	96.76	56.10	69.87	65.53	78.51
		Maha	99.48	99.72	93.51	96.92	73.32	85.23	83.00	91.68
		OCSVM	99.63	99.86	91.70	95.79	71.69	84.17	83.17	91.24
		EAD	99.63	99.78	98.22	99.26	76.58	86.34	88.26	94.08
	SVHN	LID	94.52	97.84	83.46	90.78	86.60	92.31	79.46	88.16
		Maha	97.90	99.60	92.22	97.16	93.04	95.74	84.95	92.13
		OCSVM	98.06	99.64	95.91	98.12	92.15	95.58	89.19	93.29
		EAD	98.33	99.69	96.80	98.59	93.70	96.18	90.66	94.62

Table 2: **Comparative assessment of EAD and competing methods.** Performance comparison of the EAD, LID [19], Mahalanobis [18], OCSVM detectors (all the pairwise combinations of the three single detectors are available in Supplementary Table 5). The Table contains the AUROC and AUPR for all the combinations of selected datasets (CIFAR-10, CIFAR-100 and SVHN), models (DenseNet and ResNet), and attacks (FGSM, BIM, DeepFool and CW). See Methods for further details.

ficient detectors, such as Mahalanobis and LID, and which showed satisfactory performances on tests (see Supplementary Table 5).

A second limitation is related to the properties of the logistic classifier employed to combine layer- and detector-specific scores. As shown above, the effectiveness of the detectors and the importance of the layers is closely related to the attack type, and result in different optimal weights of the logit. As a consequence, in case of unknown attacks, the selection of weights may be complex or even unfeasible, possibly impacting the detector performance, as shown in the related experiment. Thus, alternative strategies to combine scores and/or detectors might be considered to improve the generability of our approach, e.g. via weighted averaging or voting schemes [64], as well as via the exploitation of more robust feature selection and classification strategies.

6 Discussion and Conclusions

We introduced the EAD ensemble approach for adversarial detection, motivated by the observation that distinct detectors are able to isolate non-overlapping subsets of adversarial examples, by exploiting different properties of the input data in the internal representation of a DNN. Accordingly,

the integration of layer-specific scores extracted from three independent detectors (LID, Mahalanobis and OCSVM) allows EAD to achieve significantly improved performance on benchmark datasets, models and attacks, with respect to the state-of-the-art.

It is also worth of note that the newly introduced OCSVM detector proved highly effective as stand-alone in our tests, indicating that the use of one-class classifiers for this specific task deserves an in-depth exploration.

The theoretical framework of EAD is general, hence it might be extended to include different scores, generated via any arbitrary set of independent algorithmic strategies. In this regard, it might be sound to integrate detectors processing hidden layer features with others processing the properties of the output, and which have already proven their effectiveness in adversarial detection (see, e.g. [44, 51, 48]).

Similarly, one may explore the possibility of exploiting the information on activation paths and/or regions, as suggested in [65, 41, 66], as well as of refining the score definition by focusing on class-specific features. We leave these interesting options to future investigations.

All in all, we advocate the adoption of ensemble approaches in the broad field of adversarial example detection.

			AUROC			
Model	Dataset	Detector Attack	LID	Maha	OCSVM	EAD
DN	C10	BIM	92.97	99.59	99.49	99.74
		DeepFool	69.94	82.26	81.90	84.93
		CW	70.26	87.47	86.72	90.28
	C100	BIM	31.44	97.84	95.97	60.57
		DeepFool	70.30	77.86	77.48	79.60
		CW	72.57	85.53	84.26	85.76
	SVHN	BIM	91.38	98.22	99.14	96.02
		DeepFool	79.51	91.08	93.38	84.03
		CW	84.63	94.32	97.50	84.39
	RN	C10	BIM	93.36	97.76	99.41
DeepFool			73.91	82.78	86.37	84.89
CW			78.04	84.63	94.59	93.62
C100		BIM	46.06	95.69	94.15	96.70
		DeepFool	68.12	78.25	83.44	83.27
		CW	76.24	88.70	87.56	91.40
SVHN		BIM	85.03	95.16	96.39	92.50
		DeepFool	67.36	69.29	74.69	67.05
		CW	76.43	86.85	89.55	81.66

Table 3: **Comparative assessment in the unknown attack scenario.** Performance comparison of the EAD, LID [19], Mahalanobis [18], and OCSVM detectors when both the hyperparameter optimization and the logistic regression fit are performed on the FGSM attack. The Table contains the AUROC for all the combinations of selected datasets (CIFAR-10, CIFAR-100 and SVHN), models (DenseNet and ResNet), and attacks (BIM, DeepFool and CW). See Methods for further details.

References

- [1] A. Krizhevsky, I. Sutskever, and G. E. Hinton, “ImageNet classification with deep convolutional neural networks,” *Communications of the ACM*, vol. 60, pp. 84–90, May 2017. [1](#)
- [2] K. Simonyan and A. Zisserman, “Very Deep Convolutional Networks for Large-Scale Image Recognition,” in *3rd International Conference on Learning Representations, ICLR 2015, San Diego, CA, USA, May 7-9, 2015, Conference Track Proceedings* (Y. Bengio and Y. LeCun, eds.), 2015. [1](#)
- [3] G. Hinton, L. Deng, D. Yu, G. E. Dahl, A.-r. Mohamed, N. Jaitly, A. Senior, V. Vanhoucke, P. Nguyen, T. N. Sainath, and B. Kingsbury, “Deep neural networks for acoustic modeling in speech recognition: The shared views of four research groups,” *IEEE Signal Processing Magazine*, vol. 29, no. 6, pp. 82–97, 2012. [1](#)
- [4] D. Bahdanau, K. Cho, and Y. Bengio, “Neural machine translation by jointly learning to align and translate,” in *3rd International Conference on Learning Representations, ICLR 2015, San Diego, CA, USA, May 7-9, 2015, Conference Track Proceedings* (Y. Bengio and Y. LeCun, eds.), 2015. [1](#)
- [5] Y. Kim, “Convolutional neural networks for sentence classification,” in *Proceedings of the 2014 Conference on Empirical Methods in Natural Language Processing (EMNLP)*, (Doha, Qatar), pp. 1746–1751, Association for Computational Linguistics, Oct. 2014. [1](#)
- [6] V. Mnih, K. Kavukcuoglu, D. Silver, A. A. Rusu, J. Veness, M. G. Bellemare, A. Graves, M. A. Riedmiller, A. Fidjeland, G. Ostrovski, S. Petersen, C. Beattie, A. Sadik, I. Antonoglou, H. King, D. Kumaran, D. Wierstra, S. Legg, and D. Hassabis, “Human-level control through deep reinforcement learning,” *Nat.*, vol. 518, no. 7540, pp. 529–533, 2015. [1](#)
- [7] D. Silver, A. Huang, C. J. Maddison, A. Guez, L. Sifre, G. van den Driessche, J. Schrittwieser, I. Antonoglou, V. Panneershelvam, M. Lanctot, S. Dieleman, D. Grewe, J. Nham, N. Kalchbrenner, I. Sutskever, T. P. Lillicrap, M. Leach, K. Kavukcuoglu, T. Graepel, and D. Hassabis, “Mastering the game of Go with deep neural networks and tree search,” *Nat.*, vol. 529, no. 7587, pp. 484–489, 2016. [1](#)
- [8] C. Angermueller, T. Pärnamaa, L. Parts, and O. Stegle, “Deep learning for computational biology,” *Molecular systems biology*, vol. 12, no. 7, p. 878, 2016. [1](#)
- [9] A. W. Senior, R. Evans, J. Jumper, J. Kirkpatrick, L. Sifre, T. Green, C. Qin, A. Zidek, A. W. R. Nelson, A. Bridgland, H. Penedones, S. Petersen, K. Simonyan, S. Crossan, P. Kohli, D. T. Jones, D. Silver, K. Kavukcuoglu, and D. Hassabis, “Improved protein structure prediction using potentials from deep learning,” *Nat.*, vol. 577, no. 7792, pp. 706–710, 2020. [1](#)
- [10] C. Szegedy, W. Zaremba, I. Sutskever, J. Bruna, D. Erhan, I. Goodfellow, and R. Fergus, “Intriguing properties of neural networks,” in *International Conference on Learning Representations*, 2014. [1](#)
- [11] I. Goodfellow, J. Shlens, and C. Szegedy, “Explaining and harnessing adversarial examples,” in *International Conference on Learning Representations*, 2015. [1, 2, 3](#)
- [12] B. Kolosnjaji, A. Demontis, B. Biggio, D. Maiorca, G. Giacinto, C. Eckert, and F. Roli, “Adversarial malware binaries: Evading deep learning for malware detection in executables,” in *26th European Signal Processing Conference, EUSIPCO 2018, Roma, Italy, September 3-7, 2018*, pp. 533–537, IEEE, 2018. [1](#)
- [13] Y. Qin, N. Carlini, G. W. Cottrell, I. J. Goodfellow, and C. Raffel, “Imperceptible, robust, and targeted adversarial examples for automatic speech recognition,” in *Proceedings of the 36th International Conference on Machine Learning, ICML 2019, 9-15 June 2019, Long Beach, California, USA* (K. Chaudhuri and R. Salakhutdinov, eds.), vol. 97 of *Proceedings of Machine Learning Research*, pp. 5231–5240, PMLR, 2019. [1](#)
- [14] X. Ma, Y. Niu, L. Gu, Y. Wang, Y. Zhao, J. Bailey, and F. Lu, “Understanding adversarial attacks on deep learning based medical image analysis systems,” *Pattern Recognition*, vol. 110, p. 107332, 2021. [1](#)
- [15] F. Tramèr, A. Kurakin, N. Papernot, I. J. Goodfellow, D. Boneh, and P. D. McDaniel, “Ensemble adversarial training: Attacks and defenses,” in *6th International Conference*

- on Learning Representations, ICLR 2018, Vancouver, BC, Canada, April 30 - May 3, 2018, Conference Track Proceedings, OpenReview.net, 2018. 1
- [16] N. Papernot, P. D. McDaniel, X. Wu, S. Jha, and A. Swami, “Distillation as a defense to adversarial perturbations against deep neural networks,” in *IEEE Symposium on Security and Privacy, SP 2016, San Jose, CA, USA, May 22-26, 2016*, pp. 582–597, IEEE Computer Society, 2016. 1
- [17] C. C. Aggarwal and S. Sathe, *Outlier Ensembles - an Introduction*. Springer, 2017. 2
- [18] K. Lee, K. Lee, H. Lee, and J. Shin, “A simple unified framework for detecting out-of-distribution samples and adversarial attacks,” in *Advances in Neural Information Processing Systems 31: Annual Conference on Neural Information Processing Systems 2018, NeurIPS 2018, December 3-8, 2018, Montréal, Canada* (S. Bengio, H. M. Wallach, H. Larochelle, K. Grauman, N. Cesa-Bianchi, and R. Garnett, eds.), pp. 7167–7177, 2018. 2, 3, 4, 5, 6, 8, 9
- [19] X. Ma, B. Li, Y. Wang, S. M. Erfani, S. N. R. Wijewickrema, G. Schoenebeck, D. Song, M. E. Houle, and J. Bailey, “Characterizing adversarial subspaces using local intrinsic dimensionality,” in *6th International Conference on Learning Representations, ICLR 2018, Vancouver, BC, Canada, April 30 - May 3, 2018, Conference Track Proceedings*, OpenReview.net, 2018. 2, 3, 5, 8, 9
- [20] B. Schölkopf, R. C. Williamson, A. J. Smola, J. Shawe-Taylor, and J. C. Platt, “Support vector method for novelty detection,” in *Advances in Neural Information Processing Systems 12, [NIPS Conference, Denver, Colorado, USA, November 29 - December 4, 1999]* (S. A. Solla, T. K. Leen, and K.-R. Müller, eds.), pp. 582–588, The MIT Press, 1999. 2, 4
- [21] S. Ma, Y. Liu, G. Tao, W.-C. Lee, and X. Zhang, “NIC: Detecting adversarial samples with neural network invariant checking,” in *26th Annual Network and Distributed System Security Symposium, NDSS 2019, San Diego, California, USA, February 24-27, 2019*, The Internet Society, 2019. 2, 3, 4
- [22] K. He, X. Zhang, S. Ren, and J. Sun, “Deep residual learning for image recognition,” in *Proceedings of the IEEE Conference on Computer Vision and Pattern Recognition (CVPR)*, June 2016. 2
- [23] G. Huang, Z. Liu, L. Van Der Maaten, and K. Q. Weinberger, “Densely connected convolutional networks,” in *Proceedings of the IEEE Conference on Computer Vision and Pattern Recognition*, pp. 4700–4708, 2017. 2
- [24] A. Krizhevsky, “Learning Multiple Layers of Features from Tiny Images.” 2
- [25] Y. Netzer, T. Wang, A. Coates, A. Bissacco, B. Wu, and A. Y. Ng, “Reading digits in natural images with unsupervised feature learning,” in *NIPS Workshop on Deep Learning and Unsupervised Feature Learning 2011*, 2011. 2
- [26] A. Kurakin, I. J. Goodfellow, and S. Bengio, “Adversarial examples in the physical world,” in *5th International Conference on Learning Representations, ICLR 2017, Toulon, France, April 24-26, 2017, Workshop Track Proceedings*, OpenReview.net, 2017. 2, 3
- [27] S.-M. Moosavi-Dezfooli, A. Fawzi, and P. Frossard, “DeepFool: A simple and accurate method to fool deep neural networks,” in *2016 IEEE Conference on Computer Vision and Pattern Recognition, CVPR 2016, Las Vegas, NV, USA, June 27-30, 2016*, pp. 2574–2582, IEEE Computer Society, 2016. 2, 3
- [28] N. Carlini and D. A. Wagner, “Adversarial examples are not easily detected: Bypassing ten detection methods,” in *Proceedings of the 10th ACM Workshop on Artificial Intelligence and Security, AISec@CCS 2017, Dallas, TX, USA, November 3, 2017* (B. M. Thuraisingham, B. Biggio, D. M. Freeman, B. Miller, and A. Sinha, eds.), pp. 3–14, ACM, 2017. 2
- [29] D. Hendrycks and K. Gimpel, “Early methods for detecting adversarial images,” in *5th International Conference on Learning Representations, ICLR 2017, Toulon, France, April 24-26, 2017, Workshop Track Proceedings*, OpenReview.net, 2017. 3
- [30] K. Grosse, P. Manoharan, N. Papernot, M. Backes, and P. D. McDaniel, “On the (statistical) detection of adversarial examples,” *CoRR*, vol. abs/1702.06280, 2017. 3
- [31] F. Carrara, F. Falchi, R. Caldelli, G. Amato, R. Fumarola, and R. Becarelli, “Detecting adversarial example attacks to deep neural networks,” in *Proceedings of the 15th International Workshop on Content-Based Multimedia Indexing, CBMI 2017, Florence, Italy, June 19-21, 2017*, pp. 38:1–38:7, ACM, 2017. 3
- [32] N. Papernot and P. McDaniel, “Deep k-Nearest Neighbors: Towards Confident, Interpretable and Robust Deep Learning,” *arXiv:1803.04765 [cs, stat]*, Mar. 2018. 3
- [33] G. Cohen, G. Sapiro, and R. Giryes, “Detecting adversarial samples using influence functions and nearest neighbors,” in *2020 IEEE/CVF Conference on Computer Vision and Pattern Recognition, CVPR 2020, Seattle, WA, USA, June 13-19, 2020*, pp. 14441–14450, IEEE, 2020. 3
- [34] A. Abusnaina, Y. Wu, S. Arora, Y. Wang, F. Wang, H. Yang, and D. Mohaisen, “Adversarial example detection using latent neighborhood graph,” in *Proceedings of the IEEE/CVF International Conference on Computer Vision (ICCV)*, pp. 7687–7696, Oct. 2021. 3
- [35] F. Carrara, R. Becarelli, R. Caldelli, F. Falchi, and G. Amato, “Adversarial examples detection in features distance spaces,” in *Computer Vision - ECCV 2018 Workshops - Munich, Germany, September 8-14, 2018, Proceedings, Part II* (L. Leal-Taixé and S. Roth, eds.), vol. 11130 of *Lecture Notes in Computer Science*, pp. 313–327, Springer, 2018. 3
- [36] R. Kamoi and K. Kobayashi, “Why is the mahalanobis distance effective for anomaly detection?,” *CoRR*, vol. abs/2003.00402, 2020. 3, 4
- [37] Z. Zheng and P. Hong, “Robust detection of adversarial attacks by modeling the intrinsic properties of deep neural networks,” in *Advances in Neural Information Processing Systems 31: Annual Conference on Neural Information Processing Systems 2018, NeurIPS 2018, December*

- 3-8, 2018, *Montréal, Canada* (S. Bengio, H. M. Wallach, H. Larochelle, K. Grauman, N. Cesa-Bianchi, and R. Garnett, eds.), pp. 7924–7933, 2018. 3
- [38] N. A. Ahuja, I. J. Ndiour, T. Kalyanpur, and O. Tickoo, “Probabilistic modeling of deep features for out-of-distribution and adversarial detection,” *CoRR*, vol. abs/1909.11786, 2019. 3
- [39] J. H. Metzen, T. Genewein, V. Fischer, and B. Bischoff, “On detecting adversarial perturbations,” in *5th International Conference on Learning Representations, ICLR 2017, Toulon, France, April 24-26, 2017, Conference Track Proceedings*, OpenReview.net, 2017. 3
- [40] X. Li and F. Li, “Adversarial examples detection in deep networks with convolutional filter statistics,” in *IEEE International Conference on Computer Vision, ICCV 2017, Venice, Italy, October 22-29, 2017*, pp. 5775–5783, IEEE Computer Society, 2017. 3
- [41] J. Lu, T. Issaranoon, and D. A. Forsyth, “SafetyNet: Detecting and rejecting adversarial examples robustly,” in *IEEE International Conference on Computer Vision, ICCV 2017, Venice, Italy, October 22-29, 2017*, pp. 446–454, IEEE Computer Society, 2017. 3, 8
- [42] R. Feinman, R. R. Curtin, S. Shintre, and A. B. Gardner, “Detecting adversarial samples from artifacts,” *CoRR*, vol. abs/1703.00410, 2017. 3
- [43] A. Sotgiu, A. Demontis, M. Melis, B. Biggio, G. Fumera, X. Feng, and F. Roli, “Deep neural rejection against adversarial examples,” *EURASIP J. Inf. Secur.*, vol. 2020, p. 5, 2020. 3
- [44] D. Hendrycks and K. Gimpel, “A baseline for detecting misclassified and out-of-distribution examples in neural networks,” in *5th International Conference on Learning Representations, ICLR 2017, Toulon, France, April 24-26, 2017, Conference Track Proceedings*, OpenReview.net, 2017. 3, 8
- [45] W. Xu, D. Evans, and Y. Qi, “Feature squeezing: Detecting adversarial examples in deep neural networks,” in *25th Annual Network and Distributed System Security Symposium, NDSS 2018, San Diego, California, USA, February 18-21, 2018*, The Internet Society, 2018. 3
- [46] D. Meng and H. Chen, “MagNet: A two-pronged defense against adversarial examples,” in *Proceedings of the 2017 ACM SIGSAC Conference on Computer and Communications Security, CCS 2017, Dallas, TX, USA, October 30 - November 03, 2017* (B. M. Thuraisingham, D. Evans, T. Malkin, and D. Xu, eds.), pp. 135–147, ACM, 2017. 3
- [47] B. Liang, H. Li, M. Su, X. Li, W. Shi, and X. Wang, “Detecting adversarial image examples in deep neural networks with adaptive noise reduction,” *IEEE Trans. Dependable Secur. Comput.*, vol. 18, no. 1, pp. 72–85, 2021. 3
- [48] K. Roth, Y. Kilcher, and T. Hofmann, “The odds are odd: A statistical test for detecting adversarial examples,” in *Proceedings of the 36th International Conference on Machine Learning, ICML 2019, 9-15 June 2019, Long Beach, California, USA* (K. Chaudhuri and R. Salakhutdinov, eds.), vol. 97 of *Proceedings of Machine Learning Research*, pp. 5498–5507, PMLR, 2019. 3, 8
- [49] B. Huang, Y. Wang, and W. Wang, “Model-agnostic adversarial detection by random perturbations,” in *Proceedings of the Twenty-Eighth International Joint Conference on Artificial Intelligence, IJCAI 2019, Macao, China, August 10-16, 2019* (S. Kraus, ed.), pp. 4689–4696, ijcai.org, 2019. 3
- [50] F. Zuo and Q. Zeng, “Exploiting the sensitivity of L2 adversarial examples to erase-and-restore,” in *ASIA CCS ’21: ACM Asia Conference on Computer and Communications Security, Virtual Event, Hong Kong, June 7-11, 2021* (J. Cao, M. H. Au, Z. Lin, and M. Yung, eds.), pp. 40–51, ACM, 2021. 3
- [51] S. Liang, Y. Li, and R. Srikant, “Enhancing the reliability of out-of-distribution image detection in neural networks,” in *6th International Conference on Learning Representations, ICLR 2018, Vancouver, BC, Canada, April 30 - May 3, 2018, Conference Track Proceedings*, OpenReview.net, 2018. 3, 5, 8
- [52] J. Aigrain and M. Detyniecki, “Detecting adversarial examples and other misclassifications in neural networks by introspection,” *CoRR*, vol. abs/1905.09186, 2019. 3
- [53] J. Lust and A. P. Condurache, “GraN: An efficient gradient-norm based detector for adversarial and misclassified examples,” in *28th European Symposium on Artificial Neural Networks, Computational Intelligence and Machine Learning, ESANN 2020, Bruges, Belgium, October 2-4, 2020*, pp. 7–12, 2020. 3
- [54] J. Monteiro, I. Albuquerque, Z. Akhtar, and T. H. Falk, “Generalizable adversarial examples detection based on bi-model decision mismatch,” in *2019 IEEE International Conference on Systems, Man and Cybernetics, SMC 2019, Bari, Italy, October 6-9, 2019*, pp. 2839–2844, IEEE, 2019. 3
- [55] H. Xu, Y. Ma, H.-C. Liu, D. Deb, H. Liu, J.-L. Tang, and A. K. Jain, “Adversarial attacks and defenses in images, graphs and text: A review,” *International Journal of Automation and Computing*, vol. 17, no. 2, pp. 151–178, 2020. 3
- [56] N. Carlini and D. A. Wagner, “Towards evaluating the robustness of neural networks,” in *2017 IEEE Symposium on Security and Privacy, SP 2017, San Jose, CA, USA, May 22-26, 2017*, pp. 39–57, IEEE Computer Society, 2017. 3
- [57] D. Tax, *One-class classification; concept-learning in the absence of counter-examples*. PhD thesis, Delft University of Technology, 2001. 4
- [58] A. Kessy, A. Lewin, and K. Strimmer, “Optimal whitening and decorrelation,” *The American Statistician*, vol. 72, no. 4, pp. 309–314, 2018. 4
- [59] J. Snoek, H. Larochelle, and R. P. Adams, “Practical bayesian optimization of machine learning algorithms,” in *Advances in Neural Information Processing Systems 25: 26th Annual Conference on Neural Information Processing Systems 2012. Proceedings of a Meeting Held December 3-6, 2012, Lake Tahoe, Nevada, United States* (P. L. Bartlett, F. C. N. Pereira, C. J. C. Burges, L. Bottou, and K. Q. Weinberger, eds.), pp. 2960–2968, 2012. 4
- [60] C. C. Aggarwal, *Linear Algebra and Optimization for Machine Learning - A Textbook*, pp. 327–329. Springer, 2020. 4

- [61] S. Alam, S. K. Sonbhadra, S. Agarwal, and P. Nagabhushan, "One-class support vector classifiers: A survey," *Knowl. Based Syst.*, vol. 196, p. 105754, 2020. 4
- [62] T. Head, M. Kumar, H. Nahrstaedt, G. Louppe, and I. Shcherbatyi, "Scikit-optimize: Sequential model-based optimization in Python." 4, 6
- [63] J. Davis and M. Goadrich, "The relationship between precision-recall and ROC curves," in *Machine Learning, Proceedings of the Twenty-Third International Conference (ICML 2006), Pittsburgh, Pennsylvania, USA, June 25-29, 2006* (W. W. Cohen and A. W. Moore, eds.), vol. 148 of *ACM International Conference Proceeding Series*, pp. 233–240, ACM, 2006. 6
- [64] Z.-H. C. scientist)Zhou, *Ensemble Methods : Foundations and Algorithms*. Chapman & Hall/CRC Machine Learning & Pattern Recognition Series, Boca Raton: CRC Press, 2012. 8
- [65] G. F. Montufar, R. Pascanu, K. Cho, and Y. Bengio, "On the number of linear regions of deep neural networks," *Advances in Neural Information Processing Systems*, vol. 27, pp. 2924–2932, 2014. 8
- [66] F. Craighero, F. Angaroni, A. Graudenzi, F. Stella, and M. Antonioti, "Investigating the compositional structure of deep neural networks," in *International Conference on Machine Learning, Optimization, and Data Science*, pp. 322–334, Springer, 2020. 8

[Supplementary Material]

EAD: an ensemble approach to detect adversarial examples from the hidden features of deep neural networks

Francesco Craighero¹, Fabrizio Angaroni¹, Fabio Stella¹, Chiara Damiani², Marco Antoniotti^{1,3}, and Alex Graudenzi^{3,4,†}

¹Dept. of Informatics, Systems and Communication, Univ. of Milan-Bicocca, Milan, Italy

²Dept. of Biotechnology and Biosciences, Univ. of Milan-Bicocca, Milan, Italy

³Bicocca Bioinformatics Biostatistics and Bioimaging Centre – B4, Milan, Italy

⁴Inst. of Molecular Bioimaging and Physiology, Consiglio Nazionale delle Ricerche (IBFM-CNR), Segrate, Milan, Italy

[†]Corresponding author

f.craighero@campus.unimib.it, alex.graudenzi@ibfm.cnr.it

{fabrizio.angaroni, fabio.stella, chiara.damiani, marco.antoniotti}@unimib.it

Contents

1 Additional Materials and Methods	1
1.1 Description of attack algorithms	1
1.2 Performance metrics	1
2 Additional results	2
2.1 Hyperparameters optimization	2
2.2 Additional comparisons of stand-alone detectors	2
2.3 Computation time	2

1 Additional Materials and Methods

1.1 Description of attack algorithms

In the following, we describe the adversarial attacks that were employed in our experiments, namely FGSM [1], BIM [2], DeepFool [3] and CW [4]:

- FGSM [1] defines optimal L_∞ constrained perturbations as:

$$\tilde{x} = x + \epsilon \cdot \text{sign}(\nabla_x J(x, t)),$$

such that ϵ is the minimal perturbation in the direction of the gradient that changes the prediction of the model from the true class y to the target class t .

- BIM [2] extends FGSM by applying it k times with a fixed step size α , while also ensuring that each perturbation remains in the ϵ -neighbourhood of the original

image x by using a per-pixel clipping function clip:

$$\tilde{x}_0 = x$$

$$\tilde{x}_{n+1} = \text{clip}_{x,\epsilon}(x_n + \alpha \cdot \text{sign}(\nabla_{\tilde{x}_n} J(\tilde{x}_n, t)))$$

- DeepFool [3] iteratively finds the optimal L_2 perturbations that are sufficient to change the target class by approximating the original non-linear classifier with a linear one. Thanks to the linearization, in the binary classification setting the optimal perturbation corresponds to the distance to the (approximated) separating hyperplane, while in the multiclass the same idea is extended to a one-vs-all scheme. In practice, at each step i the method computes the optimal perturbation p_i of the simplified problem, until $\tilde{x} = x + \sum_i p_i$ is misclassified.
- the CW L_2 attack [4] uses gradient descent to minimize $\|\tilde{x} - x\|^2 + c \cdot l(\tilde{x})$, where the loss l is defined as:

$$l(x) = \max(\max\{\sigma_{\text{tgt}}(\tilde{x})^i : i \neq t\} - \sigma_{\text{tgt}}(\tilde{x})^t, -\kappa).$$

The objective of the optimization is to minimize the L_2 norm of the perturbation and to maximize the difference between the target logit $\sigma_{\text{tgt}}(\tilde{x})^t$ and the one of the next most likely class up to real valued constant κ , that models the desired confidence of the crafted adversarial.

1.2 Performance metrics

Let the positive class be the adversarial examples (adv) and the negative class be the benign examples (\overline{adv}). Then, the

correctly classified adversarial and benign examples correspond to the true positives (TP) and true negatives (TN), respectively. Conversely, the wrongly classified adversarial and benign examples are the false negatives (FN) and false positives (FP), respectively.

To evaluate the detectors performances, we employed two standard threshold independent metrics, namely AUROC and AUPR [5], and the accuracy, defined as follows:

- Area Under the Receiver Operating Characteristic curve (AUROC): the area under the curve identified by specificity = $TN/(TN+FP)$ and fall-out = $FP/(FP+TN)$.
- Area Under the Precision-Recall curve (AUPR): the area under the curve identified by precision = $TP/(TP+FP)$ and recall = $TP/(TP+FN)$.
- Accuracy = $(TP+TN)/(TP+TN+FP+FN)$.

The AUROC and AUPR were evaluated given the adversarial posterior learned by the logistic function $p(adv|X)$, where X is the set of layer-specific scores (see Methods for further details). The layer-specific scores are computed from \mathcal{L}^{valid} when the AUROC is used for hyperparameters optimization for the Mahalanobis and LID detectors, and from \mathcal{L}^{test} in all the other settings, i.e. the detectors performance evaluation. Moreover, AUROC and AUPR were also used to evaluate the performance of each detector in each layer, by consider the layer-specific scores evaluated on \mathcal{L}^{test} (see, e.g., Figure 1). Note that for the OCSVM and Mahalanobis detectors, lower values corresponds to adversarial examples, while the opposite applies for the LID detector. Finally, the accuracy was used for the Bayesian hyperparameter selection procedure [6] of the OCSVM detector (please refer to the Methods section for further details).

2 Additional results

2.1 Hyperparameters optimization

In Tables 1 and 2 are reported the best hyperparameters for the OCSVM detector and the best hyperparameters of both the Mahalanobis and LID detectors, respectively. The detailed description of the hyperparameter selection procedure for each detector can be found in the Methods section.

2.2 Additional comparisons of stand-alone detectors

In Figure 1 the layer importance of the ResNet model in all the settings is illustrated. The layer importance is evaluated by the AUROC of the layer-specific scores, i.e. M_l ,

O_l and L_l for the Mahalanobis, OCSVM and LID detectors, respectively (see above). Interestingly, the most important layer is mostly dependant on the attack type, but also on the dataset and detector type. Indeed, in the DeepFool attack the most important layer is the last one, while in the other attacks the highest values of AUROC are mainly achieved in the second and fourth layers. Moreover, for CIFAR-10 the second layer is the most important in the BIM and CW settings, while in the other attacks the most important is the fourth. Last, in the BIM attack, the LID detector behaves differently than the other detectors in all settings.

In Figure 3, we report the pairwise comparisons of all detectors on all experimental settings as contingency tables (see Results for further details). The most meaningful observations can be obtained by looking at the diagonals of the table in each configuration, in which the instances detected by either one of the two detectors are counted. The greatest differences are observed in the case of DeepFool and CW attacks, especially with respect to the LID detector, e.g. 4168 vs 7680 instances in the SVHN, CW, ResNet setting of the LID/OCSVM comparison.

In Figure 4, we show the pairwise comparisons of the layer-specific scores, i.e. M_l , O_l and L_l for the Mahalanobis, OCSVM and LID detectors, respectively, in the ResNet, CIFAR-10, DeepFool setting. The most correlated detectors appear to be the OCSVM and Mahalanobis detectors (second column), mainly in layers 2 and 4 (second and fourth row). Such correlation is likely due to the pre-processing step employed in the OCSVM detector, i.e. PCA-whitening, which is closely related (by a rotation) to the ZCA-Mahalanobis whitening that is used to compute the Mahalanobis distance [7].

2.3 Computation time

All tests were executed on a n1-standard-8 Google Cloud Platform instance, with eight quad-core Intel® Xeon® CPU (2.30GHz), 30GB of RAM and a NVIDIA Tesla® K80.

The fitting time of each parameter explored in all configurations for OCSVM is reported in Figure 2. For the computation times of the Mahalanobis and LID detectors, please refer to [8] and [9].

References

- [1] I. Goodfellow, J. Shlens, and C. Szegedy, “Explaining and harnessing adversarial examples,” in *International Conference on Learning Representations*, 2015. 1
- [2] A. Kurakin, I. J. Goodfellow, and S. Bengio, “Adversarial examples in the physical world,” in *5th International Conference on Learning Representations, ICLR 2017, Toulon, France, April 24-26, 2017, Workshop Track Proceedings*, OpenReview.net, 2017. 1

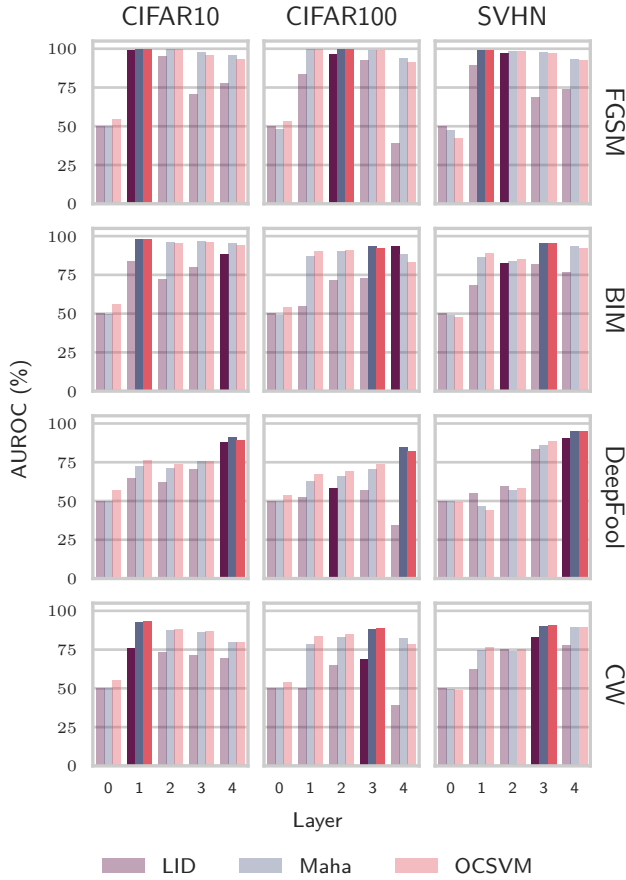


Figure 1: **Influence of layers in adversarial detection (ResNet model).** For each configuration of datasets and attacks on the ResNet model, the AUROC of each layer-specific score for OCSVM, LID and Mahalanobis detectors is returned. For each configuration and detector, the best performing layer is highlighted with a darker shade.

- [3] S.-M. Moosavi-Dezfooli, A. Fawzi, and P. Frossard, “DeepFool: A simple and accurate method to fool deep neural networks,” in *2016 IEEE Conference on Computer Vision and Pattern Recognition, CVPR 2016, Las Vegas, NV, USA, June 27-30, 2016*, pp. 2574–2582, IEEE Computer Society, 2016. [1](#)
- [4] N. Carlini and D. A. Wagner, “Towards evaluating the robustness of neural networks,” in *2017 IEEE Symposium on Security and Privacy, SP 2017, San Jose, CA, USA, May 22-26, 2017*, pp. 39–57, IEEE Computer Society, 2017. [1](#)
- [5] J. Davis and M. Goadrich, “The relationship between precision-recall and ROC curves,” in *Machine Learning, Proceedings of the Twenty-Third International Conference (ICML 2006), Pittsburgh, Pennsylvania, USA, June 25-29, 2006* (W. W. Cohen and A. W. Moore, eds.), vol. 148 of *ACM International Conference Proceeding Series*, pp. 233–240, ACM, 2006. [2](#)

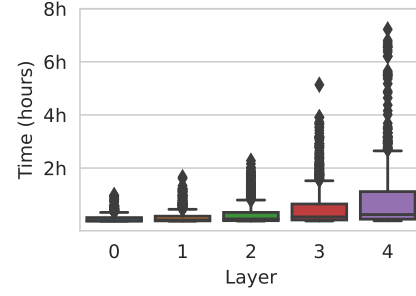
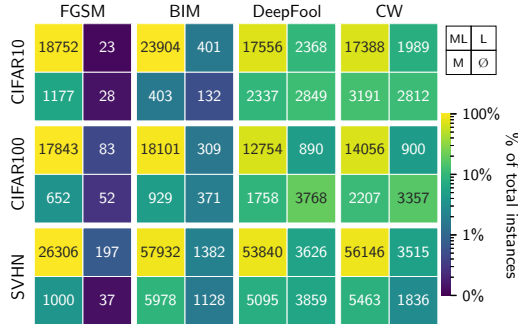
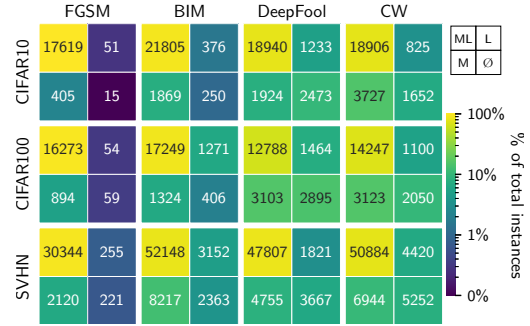


Figure 2: **OCSVM fit times by layer.** Fitting times of the OCSVM stand-alone detector, for each configuration reported in Table 1. Attack, model and dataset are aggregated, since the mean fit time depends only on the layer on which the detector was trained, i.e. the deeper the layer, the higher the mean fit time.

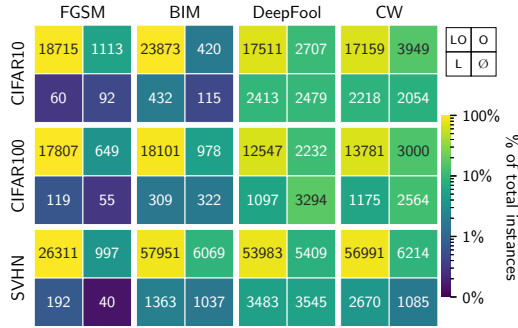
- [6] J. Snoek, H. Larochelle, and R. P. Adams, “Practical bayesian optimization of machine learning algorithms,” in *Advances in Neural Information Processing Systems 25: 26th Annual Conference on Neural Information Processing Systems 2012. Proceedings of a Meeting Held December 3-6, 2012, Lake Tahoe, Nevada, United States* (P. L. Bartlett, F. C. N. Pereira, C. J. C. Burges, L. Bottou, and K. Q. Weinberger, eds.), pp. 2960–2968, 2012. [2](#)
- [7] A. Kessy, A. Lewin, and K. Strimmer, “Optimal whitening and decorrelation,” *The American Statistician*, vol. 72, no. 4, pp. 309–314, 2018. [2](#)
- [8] K. Lee, K. Lee, H. Lee, and J. Shin, “A simple unified framework for detecting out-of-distribution samples and adversarial attacks,” in *Advances in Neural Information Processing Systems 31: Annual Conference on Neural Information Processing Systems 2018, NeurIPS 2018, December 3-8, 2018, Montréal, Canada* (S. Bengio, H. M. Wallach, H. Larochelle, K. Grauman, N. Cesa-Bianchi, and R. Garnett, eds.), pp. 7167–7177, 2018. [2, 7](#)
- [9] X. Ma, B. Li, Y. Wang, S. M. Erfani, S. N. R. Wijewickrema, G. Schoenebeck, D. Song, M. E. Houle, and J. Bailey, “Characterizing adversarial subspaces using local intrinsic dimensionality,” in *6th International Conference on Learning Representations, ICLR 2018, Vancouver, BC, Canada, April 30 - May 3, 2018, Conference Track Proceedings*, OpenReview.net, 2018. [2, 7](#)



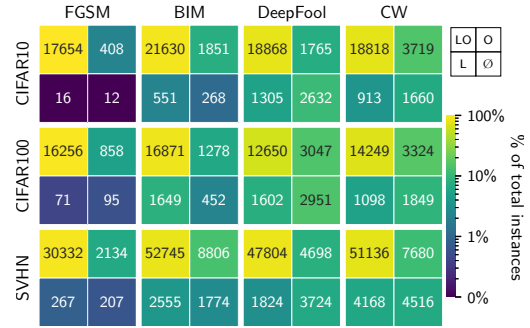
(a) LID (L) vs Mahalanobis (M), DenseNet.



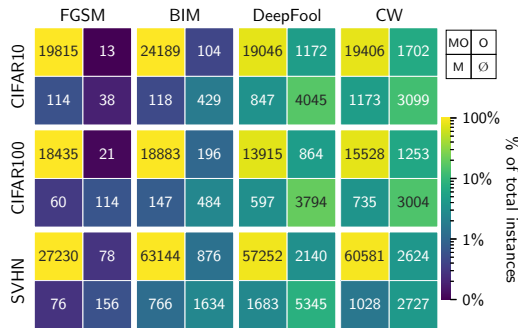
(b) LID (L) vs Mahalanobis (M), ResNet.



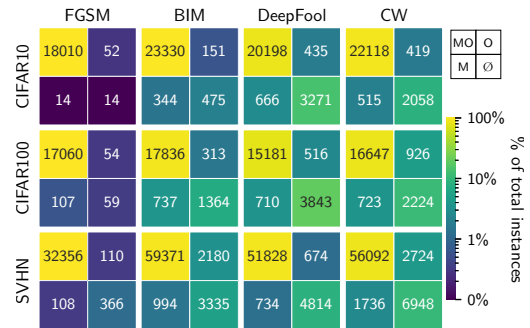
(c) LID (L) vs OCSVM (O), DenseNet.



(d) LID (L) vs OCSVM (O), ResNet.



(e) Maha (M) vs OCSVM (O), DenseNet.



(f) Maha (M) vs OCSVM (O), ResNet.

Figure 3: **Comparison of predictions of single detectors.** The contingency table shows the number of adversarial examples correctly identified: by both the detectors (top-left box), by either one of the two methods (diagonal boxes), by none of them (lower-right box), in all the experimental settings described in the main text.

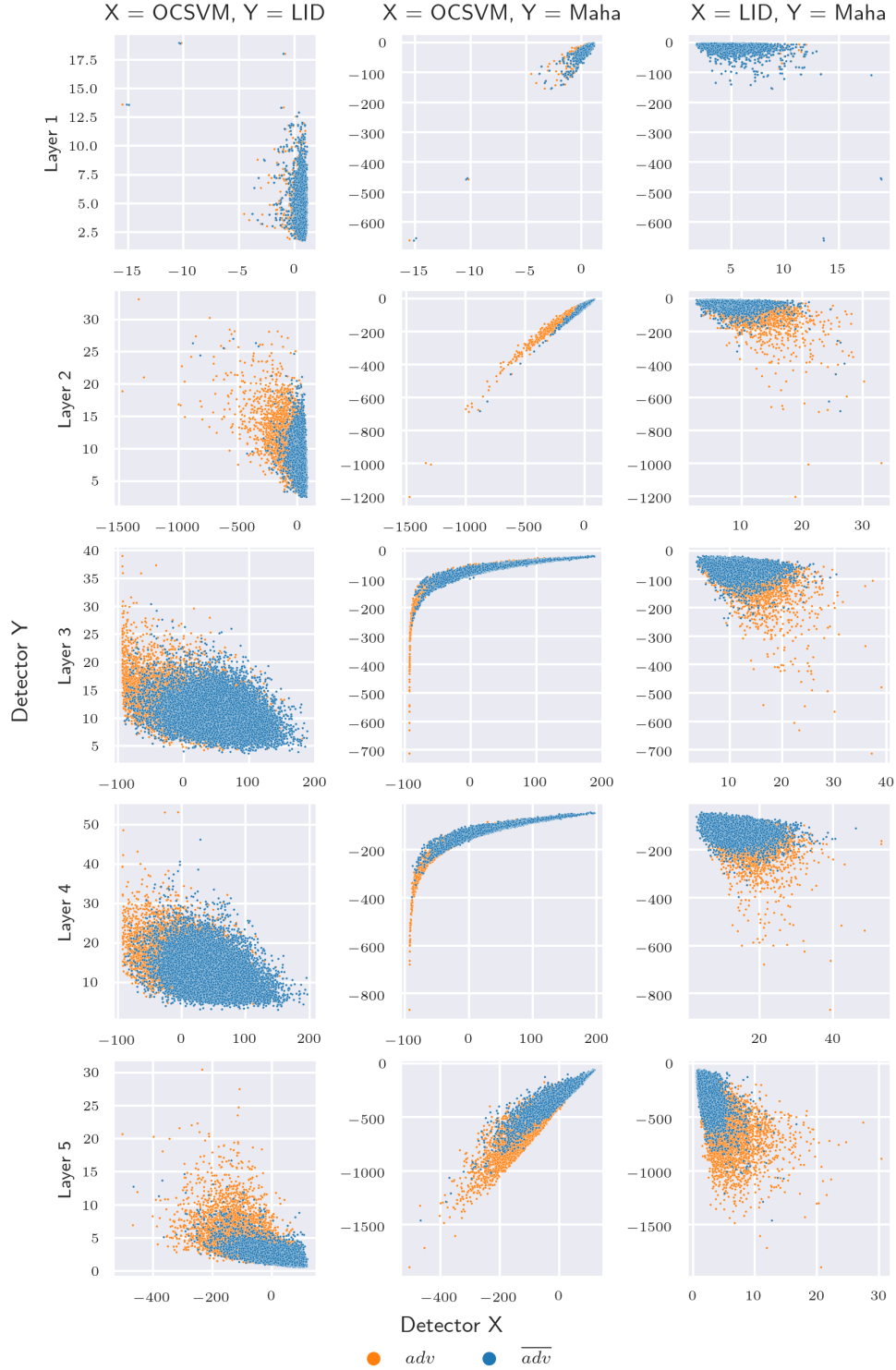


Figure 4: **Pairwise layer-specific scores comparison.** Comparison of the layer scores of OCSVM, LID and Mahalanobis detectors, i.e. O_l , L_l and M_l , respectively, for each layer l and for the Resnet, CIFAR-10, DeepFool configuration.

Model	Dataset	Layer Parameter Attack	Best Value									
			0		1		2		3		4	
			ν	γ	ν	γ	ν	γ	ν	γ	ν	γ
DenseNet	CIFAR-10	FGSM	1.27e-2	9.43e-2	7.81e-3	2.53e-4	7.81e-3	1.79e-4	2.06e-2	3.05e-5		
		BIM	9.40e-3	9.78e-3	4.15e-2	1.23e-2	1.87e-2	1.45e-2	1.26e-2	6.08e-5		
		DeepFool	1.12e-2	3.05e-5	7.81e-3	1.87e-2	1.29e-1	9.86e-5	1.23e-1	6.21e-3		
		CW	1.13e-2	1.32e-4	4.19e-2	2.86e-2	1.17e-1	1.65e-2	5.69e-2	8.62e-3		
	CIFAR-100	FGSM	8.25e-2	2.81e-4	7.81e-3	3.05e-5	7.81e-3	3.05e-5	2.04e-2	3.05e-5		
		BIM	1.41e-2	1.75e-2	7.81e-3	1.7e-2	6.17e-2	7.93e-4	2.09e-2	4.11e-3		
		DeepFool	1.10e-2	1.2e-4	8.81e-2	7.83e-3	4.67e-2	1.01e-2	1.08e-1	2.51e-4		
		CW	7.81e-3	3.05e-5	1.22e-1	9.69e-3	1.37e-1	3.35e-5	1.10e-1	3.05e-5		
	SVHN	FGSM	7.81e-3	6.1e-2	7.81e-3	2.52e-4	7.81e-3	4.88e-5	7.81e-3	3.05e-5		
		BIM	7.81e-3	2.32e-4	2.17e-2	2.98e-4	4.03e-2	7.63e-4	2.45e-2	3.05e-5		
		DeepFool	7.81e-3	3.05e-5	1.45e-2	1.74e-3	2.84e-2	3.05e-5	4.55e-2	4.16e-4		
		CW	7.81e-3	3.05e-5	1.18e-2	1.35e-2	8.92e-3	1.55e-2	1.43e-2	7.18e-3		
ResNet	CIFAR-10	FGSM	7.81e-3	3.05e-5	7.81e-3	3.05e-5	8.42e-3	7.69e-5	3.06e-2	9.42e-3	7.81e-3	2.25e-3
		BIM	7.81e-3	3.05e-5	2.95e-2	7.7e-3	4.12e-2	3.05e-5	4.09e-2	1.01e-3	1.04e-2	3.63e-3
		DeepFool	7.82e-3	3.16e-5	5.59e-2	3.50e-4	7.15e-2	9.23e-3	7.93e-2	5.22e-3	7.15e-2	4.73e-5
		CW	7.81e-3	3.05e-5	1.01e-1	5.92e-3	9.72e-2	5.53e-4	9.64e-2	9.35e-3	7.81e-3	4.6e-3
	CIFAR-100	FGSM	7.81e-3	9.77e-5	1.93e-2	3.23e-5	2.54e-2	5.58e-4	4.6e-2	1.01e-3	4.29e-2	1.28e-3
		BIM	7.81e-3	3.12e-5	1.2e-1	1.07e-3	1.29e-1	1.10e-4	6.90e-2	2.36e-3	1.18e-1	6.21e-4
		DeepFool	7.81e-3	3.05e-5	1.10e-1	3.28e-3	3.71e-2	9.03e-3	7.24e-2	3.05e-5	1.58e-1	5.43e-5
		CW	7.81e-3	3.05e-5	1.54e-2	4.32e-2	1.44e-1	3.05e-5	1.08e-1	4.46e-5	4.77e-2	2.35e-3
	SVHN	FGSM	7.81e-3	3.05e-5	2.81e-2	1.2e-4	4.36e-2	3.05e-5	5.53e-2	1.02e-3	2.03e-2	1.33e-4
		BIM	7.81e-3	3.05e-5	1.19e-1	3.76e-2	1.4e-1	1.82e-2	6.88e-2	1.18e-3	5.65e-2	1.33e-4
		DeepFool	7.81e-3	3.05e-5	7.81e-3	3.05e-5	1.78e-2	1.12e-2	1.22e-1	1.17e-3	2.4e-2	4.12e-5
		CW	7.81e-3	3.05e-5	7.81e-3	4.63e-2	1.58e-1	1.18e-2	1.09e-2	9.82e-3	4.63e-2	1.62e-4

Table 1: **Best hyperparameters for the OCSVM detector.** Optimal OCSVM hyperparameters (ν , γ) for all the combinations of layer, model (DenseNet, ResNet), dataset (CIFAR-10, CIFAR-100, SVHN) and attack (FGSM, BIM, DeepFool, CW).

Model	Dataset	Parameter Attack	Best Value	
			ϵ	k
DenseNet	CIFAR-10	FGSM	0.001	60
		BIM	0.0	90
		DeepFool	0.0	20
		CW	0.0	20
	CIFAR-100	FGSM	0.0014	90
		BIM	0.0014	90
		DeepFool	0.0	80
		CW	0.0	70
	SVHN	FGSM	0.0005	90
		BIM	0.001	80
		DeepFool	0.0005	20
		CW	0.0	20
ResNet	CIFAR-10	FGSM	0.001	80
		BIM	0.0005	90
		DeepFool	0.001	20
		CW	0.0	50
	CIFAR-100	FGSM	0.0005	90
		BIM	0.001	90
		DeepFool	0.001	80
		CW	0.001	90
	SVHN	FGSM	0.0005	80
		BIM	0.0005	30
		DeepFool	0.001	20
		CW	0.0	20

Table 2: **Best hyperparameters for Mahalanobis and LID detectors.** Optimal Mahalanobis and LID hyperparameters, i.e. perturbation magnitude ϵ and number of neighbors k , respectively, for all the combinations of method, model (DenseNet, ResNet), dataset (CIFAR-10, CIFAR-100, SVHN) and attack (FGSM, BIM, DeepFool, CW).

Model	Dataset	Attack Detector	FGSM		BIM		DeepFool		CW	
			AUPR	AUROC	AUPR	AUROC	AUPR	AUROC	AUPR	AUROC
DenseNet	CIFAR-10	LID	96.37	98.30	99.52	99.73	75.21	85.22	69.75	80.88
		Maha	99.80	99.96	99.46	99.75	74.46	82.73	78.43	87.42
		OCSVM	99.58	99.88	99.24	99.69	77.01	84.74	82.98	90.24
		Maha+LID	99.69	99.89	99.83	99.93	81.11	88.49	81.22	89.11
		OCSVM+LID	99.79	99.95	99.90	99.96	83.17	89.00	85.30	91.50
		OCSVM+Maha	99.85	99.94	99.47	99.78	79.78	86.52	83.17	90.49
		EAD	99.70	99.89	99.90	99.96	83.70	89.36	85.30	91.50
	CIFAR-100	LID	98.39	99.29	96.31	98.11	55.88	70.12	59.67	72.80
		Maha	99.49	99.87	97.64	99.10	67.79	78.49	74.99	86.86
		OCSVM	99.49	99.84	98.23	99.30	69.17	79.27	78.71	88.95
		Maha+LID	99.69	99.90	97.85	99.11	70.86	81.02	79.06	89.82
		OCSVM+LID	99.80	99.93	98.85	99.57	73.24	83.06	82.32	91.78
		OCSVM+Maha	99.62	99.89	98.15	99.37	69.71	80.07	81.37	90.20
		EAD	99.78	99.93	98.37	99.47	73.05	83.07	83.40	92.15
	SVHN	LID	98.59	99.07	92.13	94.79	85.80	91.83	90.47	94.61
		Maha	99.45	99.85	97.93	99.26	90.00	94.93	90.95	97.16
		OCSVM	99.51	99.86	97.38	99.17	91.40	95.00	96.54	98.50
		Maha+LID	99.80	99.93	98.64	99.50	92.15	95.65	95.29	98.32
		OCSVM+LID	99.81	99.93	98.45	99.44	92.63	95.58	98.21	99.19
		OCSVM+Maha	99.54	99.87	98.50	99.42	92.38	95.66	96.97	98.65
		EAD	99.83	99.91	98.93	99.57	93.27	96.04	98.13	99.16
ResNet	CIFAR-10	LID	99.18	99.67	94.37	96.50	79.40	88.58	73.95	82.29
		Maha	99.87	99.90	99.06	99.58	85.64	91.60	92.28	95.90
		OCSVM	99.99	99.99	98.95	99.44	83.90	90.83	92.26	95.68
		Maha+LID	99.97	99.98	99.45	99.73	86.40	92.26	92.53	96.07
		OCSVM+LID	99.99	99.99	99.54	99.75	85.36	91.71	92.81	96.08
		OCSVM+Maha	99.99	99.99	99.34	99.67	87.95	92.45	93.24	96.36
		EAD	99.99	99.99	99.58	99.78	87.77	92.89	93.35	96.46
	CIFAR-100	LID	97.53	98.78	94.52	96.76	56.10	69.87	65.53	78.51
		Maha	99.48	99.72	93.51	96.92	73.32	85.23	83.00	91.68
		OCSVM	99.63	99.86	91.70	95.79	71.69	84.17	83.17	91.24
		Maha+LID	99.58	99.79	97.63	98.94	74.66	85.65	83.56	92.50
		OCSVM+LID	99.21	99.65	98.24	99.13	73.64	85.18	84.43	92.74
		OCSVM+Maha	99.63	99.78	94.48	97.63	76.24	85.74	87.16	93.01
		EAD	99.63	99.78	98.22	99.26	76.58	86.34	88.26	94.08
	SVHN	LID	94.52	97.84	83.46	90.78	86.60	92.31	79.46	88.16
		Maha	97.90	99.60	92.22	97.16	93.04	95.74	84.95	92.13
		OCSVM	98.06	99.64	95.91	98.12	92.15	95.58	89.19	93.29
		Maha+LID	98.05	99.66	93.71	97.74	93.52	96.09	87.43	93.60
		OCSVM+LID	98.12	99.69	96.84	98.58	93.03	95.96	90.88	94.59
		OCSVM+Maha	98.39	99.68	95.83	98.14	93.48	96.00	89.19	93.41
		EAD	98.33	99.69	96.80	98.59	93.70	96.18	90.66	94.62

Figure 5: **Comparative assessment of EAD and competing methods.** Performance comparison of the EAD, LID [9], Mahalanobis [8], OCSVM detectors, and of the pairwise integration of the three single detectors. The table returns the AUROC and AUPR for all the combinations of selected datasets (CIFAR-10, CIFAR-100 and SVHN), models (DenseNet and ResNet), and attacks (FGSM, BIM, DeepFool and CW). See Methods for further details.